Computer Physics Communications 227 (2018) 1–7

Contents lists available at ScienceDirect

Computer Physics Communications

journal homepage: www.elsevier.com/locate/cpc

Influence of the confinement potential on the size-dependent optical response of metallic nanometric particles

Mario Zapata-Herrera [a], Ángela S. Camacho [b], Hanz Y. Ramírez [c,*]

[a] Materials Physics Center CSIC-UPV/EHU and Donostia International Physics Center DIPC, Donostia-San Sebastián 20018, Spain
[b] Departamento de Física, Universidad de los Andes, Bogotá, D.C. 111711, Colombia
[c] Grupo de Física Teórica y Computacional, Escuela de Física, Universidad Pedagógica y Tecnológica de Colombia (UPTC), Tunja, 150003 Boyacá, Colombia

ARTICLE INFO

Article history:
Received 24 October 2017
Received in revised form 10 February 2018
Accepted 13 February 2018
Available online 19 February 2018

Keywords:
Nanosplasmonics
Quantum effects
Field enhancement factor
Finite element method

ABSTRACT

In this paper, different confinement potential approaches are considered in the simulation of size effects on the optical response of silver spheres with radii at the few nanometer scale. By numerically obtaining dielectric functions from different sets of eigenenergies and eigenstates, we simulate the absorption spectrum and the field enhancement factor for nanoparticles of various sizes, within a quantum framework for both infinite and finite potentials. The simulations show significant dependence on the sphere radius of the dipolar surface plasmon resonance, as a direct consequence of energy discretization associated to the strong confinement experienced by conduction electrons in small nanospheres. Considerable reliance of the calculated optical features on the chosen wave functions and transition energies is evidenced, so that discrepancies in the plasmon resonance frequencies obtained with the three studied models reach up to above 30%. Our results are in agreement with reported measurements and shade light on the puzzling shift of the plasmon resonance in metallic nanospheres.

1. Introduction

In the last decade, metallic nanoparticles have drawn attention because of their boundary-located excitations originated from conduction electrons, so-called Localized Surface Plasmon Resonances (LSPRs) [1–4]. Those LSPRs are widely understood in terms of collective oscillations of the conduction electron gas, and their frequencies typically lie in the terahertz range [5–7].

Considerable experimental and theoretical efforts in this energy range have been made to fully understand the physics underlying the optical response of those structures since applications encompass diverse fields such as cancer therapy [8], nanophotonic devices [9–11], biosensing [12], and catalysis [13,14], among others [15–17].

Nowadays, light absorption and scattering are well-known to depend on the material, size and shape of the nanoparticles, because of the increment of the surface to volume ratio [18–21]. However, experimental difficulties in classifying and isolating such small structures on the one hand, and the computationally demanding atomistic calculations in this regime where the number of atoms is at the order of 10^2–10^3, on the other hand, make the characterization of that dependence a challenging problem.

Regarding the size dependence of the LSPRs in metallic nanospheres, Scholl et al. reported few years ago a strongly fluctuating behavior in the 1–5 nm radius range, as observed by using Electron Energy-Loss Spectroscopy (EELS) [22]. That unexpected result was later challenged by H. Haberland [23], and Kisma et al. [24], by basically arguing that the asymptotic regime (where quantum confinement effects start being negligible) is valid for diameters as low as 2 nm or less.

In this work, we perform a computationally inexpensive method to study the optical response of silver nanoparticles in this controversial size range, articulating classical electrodynamics (pertinent because of the very high number of photons involved in the related experimental set-ups), with a quantum treatment of the conduction electrons.

We calculate dielectric functions under three different approaches for the confining potential representing the nanospheres. Significant quantitative differences among the optical responses obtained from those approaches are observed, although the results from all three models are found qualitatively consistent with the available experimental measurements.

The paper is structured as follows: In the first part, the theoretical framework underlying the calculations is provided. In the second part, we present the numerical simulation results and a discussion. Concluding remarks are drawn at the last part.

* Corresponding author.
E-mail address: hanz.ramirez@uptc.edu.co (H.Y. Ramírez).

https://doi.org/10.1016/j.cpc.2018.02.012
0010-4655/

2. Theoretical framework

We carry out the simulations in two fundamental stages: first, we obtain the dielectric function for each of the confinement models, and then we calculate two physical observables (absorption cross section and field enhancement), associated to each of those potentials.

2.1. Dielectric function

When a charge carrier is trapped in a region of size at the order of the corresponding de Broglie's wavelength (nanometric scales for conventional materials), values of energy allowed for that particle are discrete and spectral continuity cannot be considered anymore [25,26]. This is the case for conduction electrons in metallic nanospheres. That makes any classical model used in describing the electron gas response to exciting radiation, to fail at some point under reduction of the metal size. However, what that limit is, persists as a matter of debate [22,24].

Experimentally, contrastive behaviors between the 10–100 nm and the 1–10 nm regimes have been reported [22,27,28]. However, independent computational studies in that later regime are scarce because it is simultaneously too big for atomistic calculations [24], and too small for a continuous classical modeling [29].

Free electron approaches as the Drude and the hydrodynamical models, which considers the valence electrons as classical particles, are the most widely used to obtain the dielectric function of metal nanoparticles [30–35]. However, a quantum model seems more appropriate for studying electrons in nanometric structures [29,36].

In this study, we use a dielectric function first introduced by Cini and Ascarelli [37], that considers the charge carriers as quantum particles subject to spatial trapping. Accordingly, the dielectric function of a single metallic nanoparticle under the influence of an electromagnetic wave with frequency ω is given by

$$\epsilon(\omega) = \epsilon_\infty + \frac{\omega_p^2}{N} \sum_{i,f} \frac{s_{if}(F_i - F_f)}{\omega_{if}^2 - \omega^2 - i\omega\gamma_{if}}, \tag{1}$$

where ϵ_∞ is the interband contribution of core electrons, $\omega_p = \left(\frac{4\pi ne^2}{m*}\right)^{(1/2)}$ is the bulk plasmon frequency, N is the total number of conduction electrons (in silver, the same as the number of atoms in the nanoparticle), and ω_{if} and γ_{if} are respectively, the frequency and damping for a transition from an initial state i to a final state f. Temperature dependence is included through F_i and F_f which are the Fermi–Dirac distribution values for the initial and final states [27]. The oscillator strength for the transition between states $|i\rangle$ and $|f\rangle$ is defined as

$$s_{if} = \frac{2m_0\omega_{if}}{\hbar} |\langle f|z|i\rangle|^2, \tag{2}$$

where $|\langle f|z|i\rangle|$ is the corresponding transition dipole moment, under z-linearly polarized incident light [38].

Fig. 1(a) presents a schematic diagram of the excitation process and the corresponding stimulated transitions between single particle populated and unoccupied discrete energy states. This model neglects the correlation effects, which in the considered size regime are expected to exist but not to dominate. Hence, the Schrödinger equation for the electron conducting gas is solved in the non-interacting approach, i.e. in the one electron picture.

Since the eigenenergies and eigenstates of the electron are required for the calculation of the dielectric function, its particular features are expected to depend significantly on the potential used to model the carrier confinement. Then, details of the different cases studied in these calculations are presented in the next subsection.

2.2. Spherical confinement

Atomistic calculations in small silver clusters show that their shapes are well described as icosahedra or decahedra [39]. However as the particle size increases, their geometries exhibit more facets, ultimately resembling spheres [40]. According to Figure 3 in Ref. [22], for a radius larger than 1 nm, the spherical approximation fits well the nanoparticle shape.

In this work, the dielectric functions for the various studied sizes are obtained within three different approaches for the spherical confining potential, namely: (A) infinite confinement with asymptotic eigenenergies and wave functions, (B) infinite confinement with exact eigenenergies and wave functions, and (C) finite confinement with numerical eigenenergies. The first two models share the infiniteness of the potential barrier modeling the particle boundary, while the last two share the accuracy in the energy values.

2.2.1. Infinite confinement

The hard-wall spherical well is one of the few potentials with an exact known solution. Hence, given the shape of the nanostructures under study, plus the assumption of an absolutely impenetrable barrier, the wave functions and allowed energies of a conduction electron of effective mass m^* confined in a particle of radius R, are, respectively,

$$\psi_{n,l,m}(r,\theta,\phi) = \frac{1}{|j_{l+1}(\alpha_{nl})|}\sqrt{\frac{2}{R^3}} j_l\left(\frac{\alpha_{nl}}{R}r\right) Y_l^m(\theta,\phi) \tag{3}$$

and

$$E_{n,l} = \frac{\hbar^2\alpha_{ln}^2}{2m^*R^2}, \tag{4}$$

where j_l represents the lth spherical Bessel functions, Y_l^m the standard spherical harmonics, and α_{nl} the nth zero of j_l [41].

Thus, the eigenenergies and eigenfunctions of each electron in the non-interacting conduction gas are in principle fully determined, so that the necessary oscillator strengths and transition energies for the dielectric function can be obtained. However, because there is not a recurrent relation between zeros of spherical Bessel function with different l, the calculation results at last in a numerical problem.

As proposed in Ref. [22], the asymptotic approximation that provides wave functions and energies in a compact form, can be used to simplify the calculations. Within such an approximation [42], the spherical Bessel functions appearing in Eq. (3) and the eigenenergies in Eq. (4) are correspondingly reduced to

$$j_l(x) \approx \frac{1}{x}\cos\left[x - \frac{\pi}{2}(l+1)\right] \tag{5}$$

and

$$E_{n,l} = \frac{\hbar^2}{2m^*R^2}\left[\pi\left(n + \frac{l}{2} + 1\right)\right]^2. \tag{6}$$

Using the approximation given by Eqs. (5) and (6), straightforward calculation of the dielectric function can be carried out at a minimum computational cost. Nevertheless, a price is paid in accuracy because these expressions are only suitable for small l and $x \gg l^2/2 + l$ [41] [model (A)], as can be seen in Table 1, where we present a comparison between energies given by Eq. (4) with the corresponding ones from Eq. (6) for a nanoparticle of radius $R = 1$ nm. Complete agreement is observed for $l = 0$, whereas a noticeable overestimation by the approximation becomes significant as l increases.

Fig. 1(b) shows $j_l(\alpha_{ln}r/R)$ and its asymptotic approximation [Eq. (5) into Eq. (3)], as functions of the normalized radius for different values of l ($n = 1$). It is worth to note that for $l = 0$ both

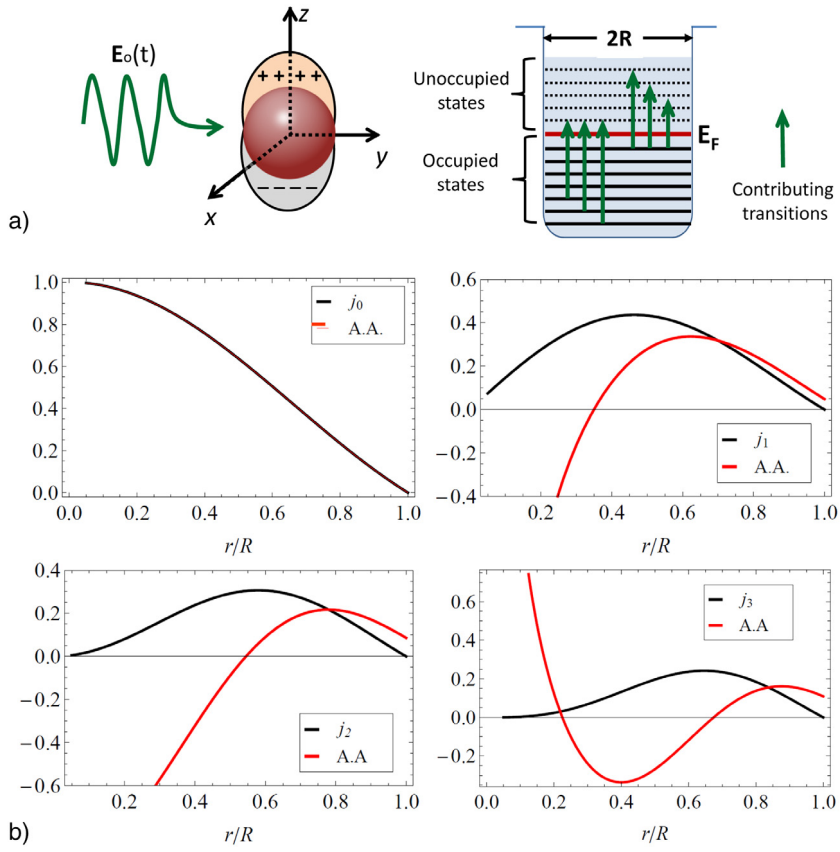

Fig. 1. (a) Schematics of the plasmon excitation and associated discrete energy transitions in the quantized system. (b) j_l and its asymptotic approximation (A.A.) as functions of the normalized position for $n = 1$ and different l's.

functions are the same, but start differing strongly as l increases. Thus, it is anticipated that model (A) will fail in quantitatively reproducing the experimental observations.

Given that spherical Bessel functions are implemented in most of the programming languages and packages, we also calculate dielectric functions by using the exact eigenstates and eigenenergies obtained from Eqs. (3) and (4) [model (B)]. In such a case, there is not analytical form for the transition energies and dipole moments, but the later can still be reduced by exploiting the azimuthal symmetry. Taking $z = r\cos\theta$ into the dipole integral

$$\langle f|z|i\rangle = \int_0^{2\pi}\int_0^{\pi}\int_0^{R} dr d\theta d\phi \; r^3 \sin\theta\cos\theta \times \Psi^*_{n_f,l_f,m_f}(r,\theta,\phi)\Psi_{n_i,l_i,m_i}(r,\theta,\phi), \tag{7}$$

this splits in angular and radial parts, which, respectively read

$$I_{ang} = \sqrt{\frac{(l_i+m_i+1)(l_i-m_i+1)}{(2l_i+1)(2l_i+3)}}\delta_{\Delta l,+1} + \sqrt{\frac{(l_i+m_i)(l_i-m_i)}{(2l_i+1)(2l_i-1)}}\delta_{\Delta l,-1} \tag{8}$$

and

$$I_{rad} = \frac{1}{|j_{l_f+1}(\alpha_{n_f l_f})|}\frac{1}{|j_{l_i+1}(\alpha_{n_i l_i})|}\left(\frac{2}{R^3}\right) \times \int_0^R dr j_{l_f}\left(\frac{\alpha_{n_f l_f}}{R}r\right) r^3 j_{l_i}\left(\frac{\alpha_{n_i l_i}}{R}r\right). \tag{9}$$

Then, the oscillator strength is different from zero only for the transitions satisfying $\Delta l = l_f - l_i = \pm 1$, as expected for plasmons coupled to photons, because of angular momentum conservation.

Beside the above selection rule, oscillator strengths in the summation of Eq. (1)are weighted by the Fermi–Dirac distribution, since initial (final) states must be occupied (empty) for a transition to contribute.

Table 1
Comparison between exact energies (upper) and asymptotically approximated energies (lower) in meV, for different values of l and n ($R = 1$ nm).

	$n=0$	$n=1$	$n=2$	$n=3$	$n=4$
$l=0$	376.03	1504.11	3384.25	6016.45	9400.71
	376.03	1504.11	3384.25	6016.45	9400.71
$l=1$	769.26	2273.77	4530.04	7538.31	11298.6
	846.64	2350.18	4606.35	7614.57	11374.9
$l=2$	1265.57	3151.57	5785.61	9170.69	13307.4
	1504.11	3384.25	6016.45	9400.71	13537.0
$l=3$	1860.45	4134.43	7148.86	10912.1	15426.0
	2350.18	4606.35	7614.57	11374.9	15887.2
$l=4$	2550.93	5219.83	8617.81	12760.9	17653.2
	3384.25	6016.45	9400.71	13537.0	18425.4
$l=5$	3334.9	6405.72	10190.75	14715.83	19987.75
	4606.35	7614.57	11374.9	15887.2	21151.69
$l=6$	4210.76	7690.4	11866.16	16775.47	22428.54
	6016.45	9400.71	13537.0	18425.4	24065.92

2.2.2. Finite confinement

Going one step further, we can use a more realistic picture considering a spherical finite binding potential to represent the electron confinement inside the nanoparticle [model (C)]. This implies to solve numerically the Schrödinger equation for the kth

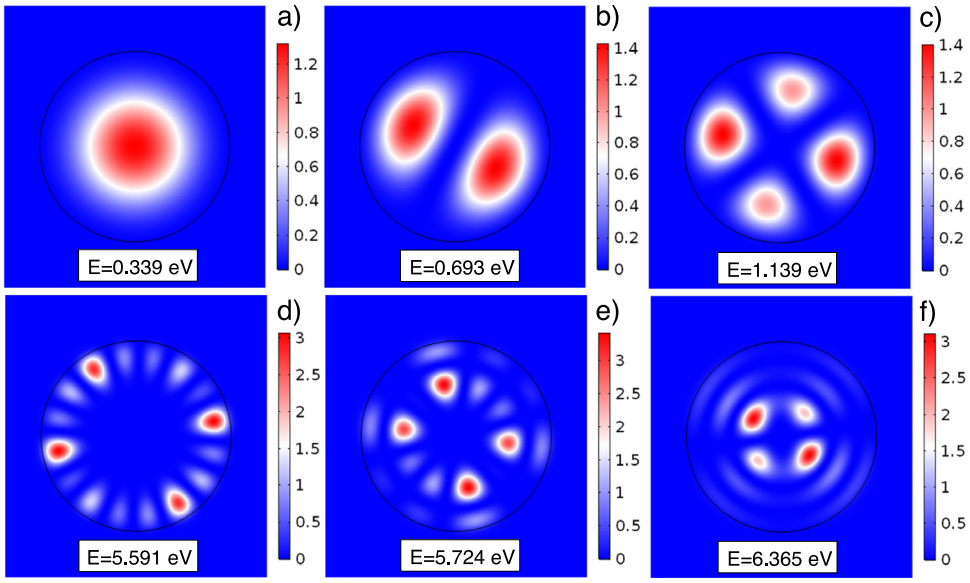

Fig. 2. Eigenenergies and the corresponding probability densities along the plane $z = 0$ of some bound states, for a confined conduction electron in a nanosphere of radius 1 nm. (a) Ground state, (b) first excited state, (c) second excited state, (d) last state before the Fermi level, (e) Fermi level, (f) first estate after the Fermi level.

quantum state, which is given by

$$\left[\frac{-\hbar^2\ \nabla^2}{2m^*} + V(r)\right]\Psi_k(r,\theta,\phi) = E_k\Psi_k(r,\theta,\phi), \tag{10}$$

where the central potential is

$$V(r) = \begin{cases} 0 & \text{if } 0 < r < R \\ V_0(R) & \text{otherwise.} \end{cases} \tag{11}$$

The well depth is related to the Fermi energy $E_F(R)$, and to the work function of the particle $W(R)$ (defined as the energy required to remove one electron from the nanoparticle), according to

$$V_0(R) = E_F(R) + W(R). \tag{12}$$

On one side, the work function is calculated following Ref. [43], so that for small particles, its size dependent value is obtained from

$$W(R) = 4.37 + \frac{5.4}{R(\text{Å})}, \tag{13}$$

where 4.37 eV is the average work function for Bulk Ag, and $5.4 = \frac{3}{8}e^2$ is a parameter that accounts for the difference in the work function for a conducting plane and a sphere.

On the other side, the Fermi energy depends specifically on the number of particles, which in turn determines the number of conduction electrons occupying the available electronic states. An initial confinement potential must be assumed to obtain states that are populated with conduction electrons following the Pauli exclusion principle, so that an *a priori* Fermi level is established. Then, such an energy $E_F^{(0)}$ is inserted into Eqs. (10) and (12), to find new eigenstates that lead to a corrected Fermi level. This process can be iteratively carried out up to find the appropriate E_F.

To obtain the *a priori* Fermi level, we start with the infinite well of previous section. The number of particles as function of the radius is estimated by fitting *ab initio* results by He et al. in Ref. [44], to the size range studied in this work. Therefore, the number of conduction electrons is taken as

$$N(R) \approx 246R^3. \tag{14}$$

In calculating oscillator strengths for the dielectric response within model (C), wave functions from model (B) were finally used, given that preliminary calculations of the pertinent dipole moments revealed differences below 1% as compared to the cases in which the corresponding numerical wave functions, at much higher computational cost, were used.

Fig. 2 shows some of the numerically obtained eigenenergies and the corresponding probability densities for a conduction electron confined in a silver nanosphere of radius $R = 1$ nm (246 atoms). The depth of the potential well in the plotted case is 11.316 eV (where an *a priori* Fermi energy $E_F^{(0)} = 6.406$ eV, was taken).

These wave function profiles evidence that the spill-out effects (electron probability density penetrating the potential barrier) are negligible, even for highly excited states.

Aiming further optimization of the calculation times, additionally to the selection rule $\Delta l = \pm 1$ from Eq. (8), transition energies with relevant contributions to the dielectric function were required to satisfy $K_BT \ll \hbar\omega_{if} \ll V_0$. In other words, not too small because of the typical temperatures at which related experiments are carried out (much lower than the Fermi temperature), and not too large because of the electromagnetic range of interest (optical frequencies).

2.3. Optical response

2.3.1. Absorption spectrum

In the studied size regime, the wavelength of the incident light is much larger than the radius of the metallic particle, and the extinction cross section reduces to the absorption component [45,46], given in terms of the dielectric function by

$$\text{Abs}(\omega) \propto \frac{\omega\epsilon_m^{3/2}\text{Im}[\epsilon(\omega)]}{c_m\ \left[(\text{Re}[\epsilon(\omega)] + 2\epsilon_m)^2 + (\text{Im}[\epsilon(\omega)])^2\right]}, \tag{15}$$

where ϵ_m is the dielectric constant of the surrounding media and c_m the light speed in that media. $\text{Re}[\epsilon(\omega)]$ and $\text{Im}[\epsilon(\omega)]$ are the real and imaginary parts of the metallic particle's dielectric function, respectively [47].

In our simulations we use $\epsilon_m = 2.5$, assuming a glass matrix embedding the silver nanospheres.

2.3.2. Field enhancement

The field enhancement factor (FEF) [29,48]is here defined as the squared norm of the ratio between the scattered electric field

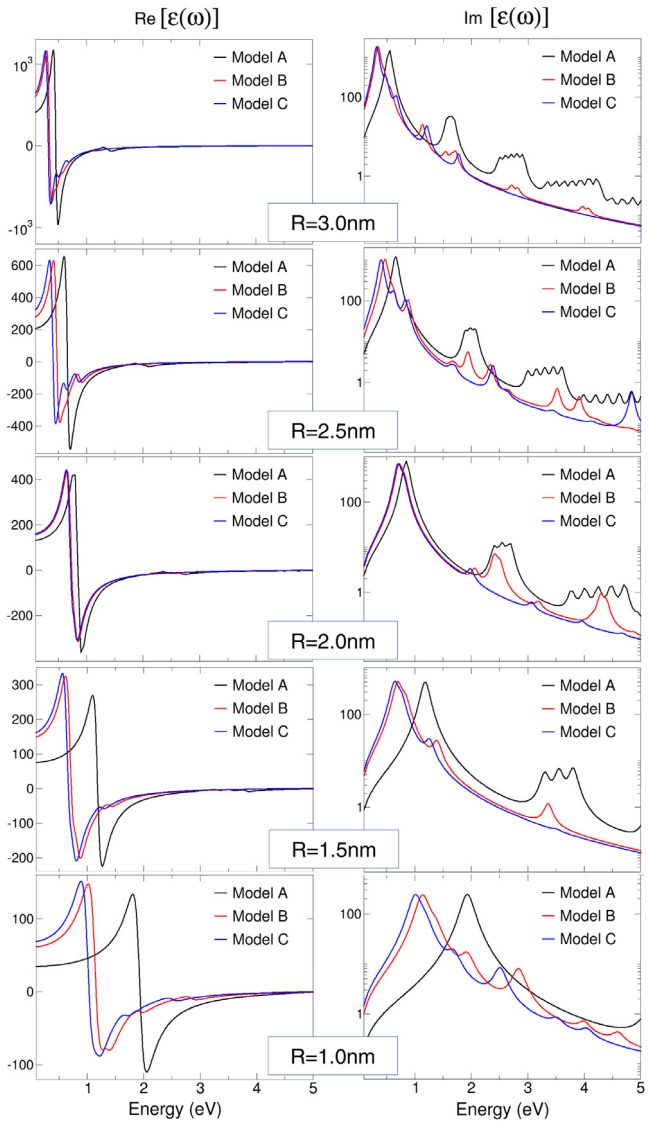

Fig. 3. Real (left) and Imaginary (right) parts of the dielectric function as functions of the exciting photon energy for silver nanoparticle of different radii, calculated with each of the three considered models. Black line → Model (A), Red line → Model (B), and Blue line → Model (C). (For interpretation of the references to color in this figure legend, the reader is referred to the web version of this article.)

calculated at the north pole of the sphere $\vec{E}_{out}$, and the amplitude of the incident z-polarized electric field $\vec{E}_{inc}$, i.e.

$$FEF = \frac{|\vec{E_{out}}|^2}{E_0^2}. \tag{16}$$

The scattered field, satisfying the Maxwell equations in material media, is obtained from the Helmholtz equation

$$\nabla^2\vec{E} - k_0^2\left(\epsilon(\omega) - \frac{i\sigma}{\omega\epsilon_0}\right)\vec{E} = 0, \tag{17}$$

where $\sigma = \frac{\omega}{4\pi i}\epsilon(\omega)$ is the nanoparticle complex conductivity and $k_0 = \omega\sqrt{\epsilon_0\mu_0}$, with ϵ_0 and μ_0 the values of permittivity and permeability in vacuum, respectively [29].

3. Results and discussion

To numerically solve the Schrödinger equation, as well as the Helmholtz equation, we use a standard finite element method (FEM), implemented in the Comsol Multiphysics Package [29,49–52], on a commercial computer with an i7 processor of 2 GHz. The typical calculation time lies in the scale of hours, instead of days and weeks, as usual for DFT jellium or atomistic simulations [24].

Along the calculations, we use the following set of standard parameters for silver, taken from Refs. [19,22,53,54]: $\epsilon_\infty = 3.66$, $m^* = 0.99\ m_0$, $\omega_p = 9.01$ eV, and $\gamma(R) = \gamma_{bulk} + \frac{A}{R}\frac{v_F}{R}$, with $\gamma_{bulk} = 2.43$ GHz, $A = 0.25$ and $v_F = 1.4 \times 10^6$ m/s.

Fig. 3 shows the real and imaginary parts of the dielectric function for silver nanospheres of different radii, calculated within the three considered models. It can be appreciated how model (A), because of the more oscillatory character of the approximated wave functions, increases the number of peaks in the imaginary part of the nanosphere dielectric response. Meanwhile models (B) and (C) present overall similar features, though a slight but consistent blue shift is observed for model (B), as compared to the one including finiteness in confinement [model (C)].

Complementarily, and distinctively for the smallest particles, the real part of the dielectric function highlights how the similarity between the results from models (B) and (C) is certainly higher than that between results from model (A) and results from any of the other two models. In other words, inaccuracies originated from the asymptotic approximation are larger than those raised from the infiniteness of the confinement potential.

In Fig. 4, the absorption spectra and enhancement factors of metallic particles are plotted for various nanosphere sizes, as functions of the exciting light energy.

Oscillations of the main resonance are observed for all three models, although the enhancement factor magnitude in model (A) evolves anomalously with size (noticeably non-monotonic behavior, whereas it is expected to increase with size). There is also an underestimation of the FEF in the results from model (A), due to spurious fluctuations of the wave functions and consequent reduced magnitude of the contributing oscillator strengths.

Resonance blue-shifts for models (A) and (B) as compared to model (C) are both evident. However, such shifts for model (A) are substantially larger than the ones for model (B). It is worth noting that the main physical reasons underlying those discrepancies are similar but not exactly the same. In model (A), the disparities are mostly related to the poorly approximated energy values of the contributing transitions with large l. On the other hand, the shifts in model (B) are originated in the bigger transition energies associated to the infiniteness of the confining potential. Then, the accuracy of the former approach is again revealed weaker than that of the later.

In Fig. 5(a), we compare the results from the different models of the LSPR energy obtained at the maximum enhancement field factor for each particle size. These are also set against the experimental data reported by Scholl et al. in Ref. [22].

In an attempt to demonstrate that fluctuation of the plasmon resonances is related to the discrete transitions considered in the dielectric function from Fig. 3, size depending energies for two of the main contributing transitions (computed within model B) are shown in Fig. 5(b). The chosen transitions were those with the lowest energies, allowed from the Fermi level [for example, in the case $R = 1$ nm, the quantum numbers of the Fermi level are $n = 1$, $l = 5$; and the numbers of the unoccupied state for the chosen transition satisfying $\Delta l = -1$ ($\Delta l = +1$) are $n = 2$, $l = 4$ ($n = 1$, $l = 6$), whose corresponding energies can be found in Table 1]. Such transition energies exhibit a non-monotonic and uncorrelated behavior, which is rooted in the fact that changes in size simultaneously modify the number of particles to be allocated in the available electronic states, and the spacing between energy levels. This makes the plasmon resonance swaying and very sensitive to slight size changes in the studied radius regime.

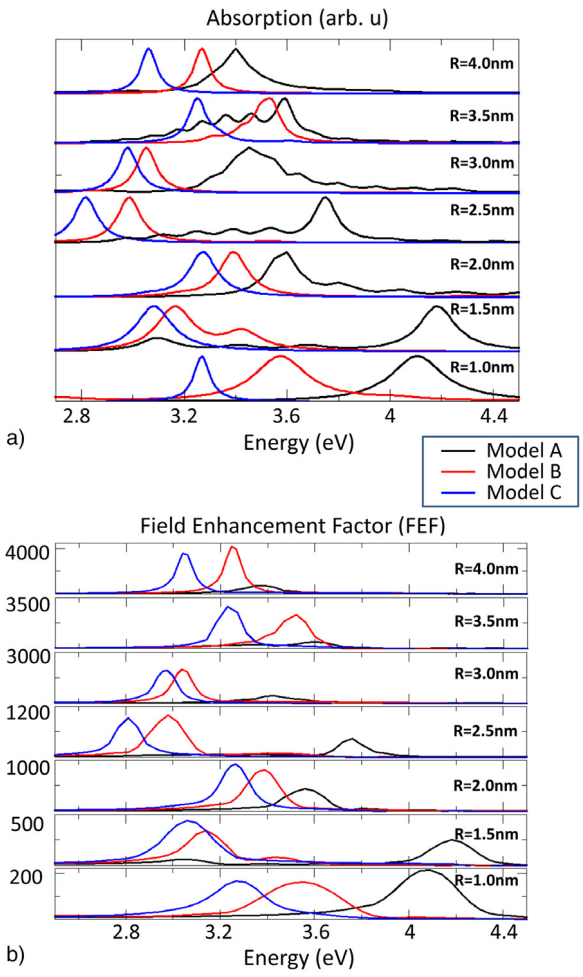

Fig. 4. (a) Normalized optical absorption and (b) FEF, as functions of the exciting photon energy, calculated within the three considered models for various nanosphere sizes. Black line → Model (A), Red line → Model (B), and Blue line → Model (C). (For interpretation of the references to color in this figure legend, the reader is referred to the web version of this article.)

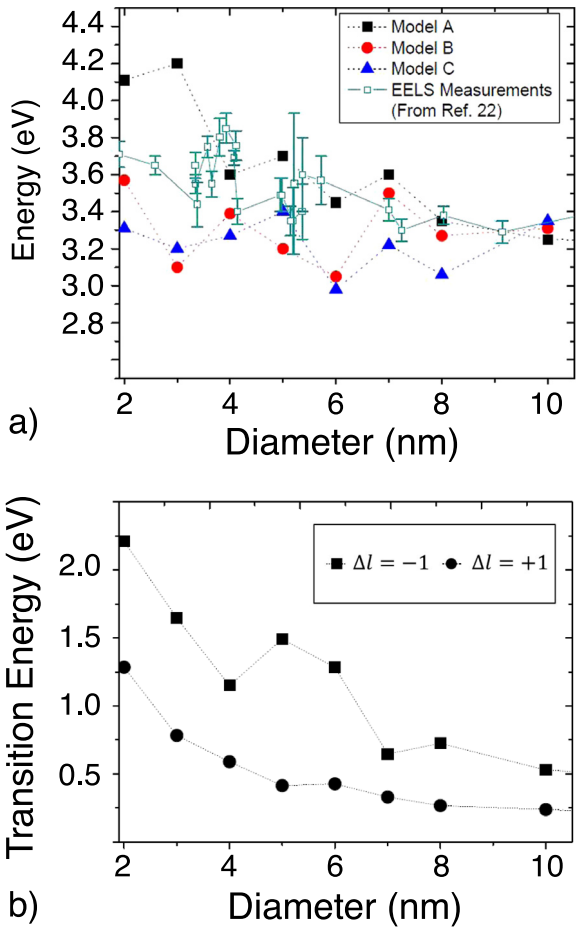

Fig. 5. (a) Plasmon energy as a function of the nanoparticle diameter. Squares, dots and triangles show the results obtained within Models (A), (B) and (C), respectively. For comparison, experimental EELS data extracted from Ref. [22] are also shown. (b) Energy transitions in model (B), of the stronger contributions from the Fermi level to unoccupied states. Squares (circles) are for the transitions satisfying $\Delta l = -1$ ($\Delta l = +1$).

Remarkably, oscillations of the absorption and FEF peaks in the studied size range are observable in all used models, as a direct consequence of including transitions between discrete energy states for the excited electron in the conduction gas. As expected, Fig. 5(a) suggests that the three models start to converge at $R = 5$ nm, where the confinement effects become negligible [28,55].

By tuning the parameter ϵ_∞, the computed data can be fitted to the proper energy range, accordingly with experimental observations, so that Fig. 5(a) displays good agreement between simulations and measured fluctuations, given that calculations include discretization of states for conduction carriers.

Furthermore, our results suggest that the measured fluctuations are not originated in the substrate neither in residual ligands [23,24], but are intrinsic to the quantum nature of the confined electron gas [29].

4. Conclusions

In this work, we simulated the optical response of ultra-small silver nanoparticles, within three confinement models, which share inclusion of discretized electron energy levels in the dielectric function. The used models differ in the eigenstates and eigenenergies employed for calculating the dipole moments and transition energies. The first model assumes infinite confinement and asymptotically approximated eigenenergies and wave functions, the second one maintains infinite confinement but considers exact solutions for eigenenergies and wave functions, and the third one considers finiteness of the confinement and uses numerically obtained eigenenergies.

For those three models, frequency dependent optical absorptions and field enhancement factors were calculated for nanospheres of various sizes, with diameters ranging from 2 nm up to 10 nm.

In the explored size regime, the computed data consistently show oscillations of the localized surface plasmon resonance energy for all the three models, being the main difference between them the magnitude of the field enhancement and the precise resonance energy for each size, whereas the swaying character of that resonance transcends the confinement particularities. This oscillating behavior can be directly related to discreteness of transitions in the electron gas, as response to the exciting electromagnetic field.

Overestimation of the plasmon resonance energies larger than 25%, along with underestimation by a factor 4 of the field enhancement, is observed under the model with infinite confinement and approximated eigenstates, as contrasted to the other two models which consider accurate eigenenergies. Comparing results from those later approaches, effects of confinement finiteness are found appreciable but not substantial, consisting of an undeviating blue

shift of around ∼5% for the model in which the potential barrier height is taken as infinite.

More generally, our results contribute to clarify the physical origin of the strong fluctuations, reported in Ref. [22], and support the interpretation according with such non-monotonic and very size-sensitive optical response relates to the quantum nature of confined conduction electrons, instead of coming from ligand presence or substrate impurities, as proposed more recently in Refs. [23,24].

Acknowledgments

The authors would like to thank financial backing. M.Z.H. acknowledges support from Colciencias through the Ph.D. studentship program no. 567, the Spanish Ministry of Economy and Competitiveness MINECO through project FIS2016-80174-P, as well as support from NIST Grant No. 70NANB15H32 of the US Department of Commerce. A.S.C. acknowledges support from the Department of Physics of the Universidad de Los Andes, and H.Y.R. acknowledges support from the Research Division of the Universidad Pedagógica y Tecnológica de Colombia (UPTC) under research grant SGI-2142.

References

[1] M.J. Puska, R.M. Nieminem, M. Manninen, Phys. Rev. B 31 (1985) 6.
[2] S.A. Maier, Plasmonics: Fundamentals and Applications, Springer, 2007.
[3] R.H. Ritchie, Phys. Rev. 106 (1957) 5.
[4] W. Ekardt, Phys. Rev. B 29 (1984) 1558.
[5] S.A. Maier, S.R. Andrews, L. Martín-Moreno, F.J. García-Vidal, Phys. Rev. Lett. 97 (2006) 176805.
[6] Z. Li, Y. Ma, R. Huang, R. Singh, J. Gu, Z. Tian, J. Han, W. Zhang, Opt. Express 19 (2011) 8912.
[7] M. Dragoman, D. Dragoman, Progr. Quant. Electr. 32 (2008) 1.
[8] X. Huang, P.K. Jain, I.H. El-Sayed, M.A. El-Sayed, Lasers Med. Sci. 23 (2008) 217.
[9] V.M. Shalaev, S. Kawata, Nanophotonics with Surface Plasmons, Elsevier, 2007.
[10] K.F. MacDonald, Z.L. Sámson, M.I. Stockman, N.I. Zheludev, Nat. Photonics 3 (2009) 55.
[11] P.G. Kik, M.L. Brongersma, Surface Plasmon Nanophotonics, in: Springer Series in Optical Sciences, Springer, 2007.
[12] J.N. Anker, W.P. Hall, O. Lyandres, N.C. Shah, J. Zhao, R.P. Van Duyne, Nat. Mater. 7 (2008) 442.
[13] X. Zhang, X. Ke, A. Du, H. Zhu, Sci. Rep. 4 (2014) 3805.
[14] S. Linic, P. Christopher, D.B. Ingram, Nat. Mater. 10 (2011) 911.
[15] E. Townsend, G.W. Bryant, Nano Lett. 12 (2012) 429.
[16] K.A. Willets, R.P. Van Duyne, Annu. Rev. Phys. Chem. 58 (2007) 267.
[17] B.K. Juluri, Y.B. Zheng, D. Ahmed, L. Jensen, T.J. Huang, J. Phys. Chem. C 112 (2008) 7309.
[18] J.C. Arias, A.S. Camacho, JEMAA 3 (2011) 11.
[19] C. Sonnichsen, Plasmons in Metal Nanostructures (Ph.D. dissertation), Munich University, 2001.
[20] Q.H. Wei, K.-H. Su, S. Durant, X. Zhang, Nano. Lett. 4 (2004) 1067.
[21] W.A. Murray, W.L. Barnes, Adv. Mat. 19 (2007) 3771.
[22] J. Scholl, A.L. Koh, J. Dionne, Nature 483 (2012) 421.
[23] H. Haberland, Nature 494 (2013) E1.
[24] M. Kuisma, A. Sakko, T.P. Rossi, A.H. Larsen, J. Enkovaara, L. Lehtovaara, T.T. Rantala, Phys. Rev. B 91 (2015) 115431.
[25] F.J. Garcia de Abajo, Nature 483 (2012) 417.
[26] M. Wubs, N.A. Mortensen, Quantum Plasmonics, in: Springer Series in Solid-State Sciences, Springer, 2017.
[27] L. Genzel, T.P. Martin, Z. Phys. B 21 (1975) 339.
[28] K.P. Charlé, L. König, S. Nepijko, I. Rabin, W. Schulze, Cryst. Res. Technol. 33 (1998) 1085.
[29] M. Zapata-Herrera, J. Flórez, A.S. Camacho, H.Y. Ramírez, Plasmonics 13 (2018) 1.
[30] K.L. Kelly, E. Coronado, L.L. Zhao, G.C. Schatz, J. Phys. Chem. B 107 (2003) 668.
[31] N.K. Grady, N.J. Halas, P. Nordlander, Chem. Phys. Lett. 399 (2004) 167.
[32] C. Noguez, J. Phys. Chem. C 111 (2007) 3806.
[33] R. Esteban, A.G. Borisov, P. Nordlander, J. Aizpurua, Nat. Commun. 3 (2012) 825.
[34] D. Muetón-Arboleda, J.M. Santillán, L.J. Mendoza-Herrera, D. Muraca, D.C. Schinca, L.B. Scaffardi, J. Phys. D 49 (2016) 075302.
[35] J. Aizpurua, R. Hillendrand, Plasmonics from Basics to Advanced Topics, in: Springer series in optical sciences, Springer, 2012.
[36] X.F. Fan, W.T. Zheng, D.J. Singh, Light-Sci. Appl. 3 (2014) e179.
[37] M. Cini, P. Ascarelli, J. Phys. F 4 (1974) 1998.
[38] H.Y. Ramírez, J. Flórez, A.S. Camacho, Phys. Chem. Chem. Phys. 17 (2015) 23938.
[39] D. Schooss, M. Blom, J. Parks, B. von Issendorff, H. Haberland, M. Kappes, Nano Lett. 5 (2005) 1972.
[40] F. Baletto, R. Ferrando, A. Fortunelli, F. Montalenti, C. Mottet, J. Chem. Phys. 116 (2002) 3856.
[41] G.B. Arfken, H.J. Weber, Mathematical Methods for Physicists, Harcourt/Academic Press, 2001.
[42] M. Abramowitz, I.A. Stegun, Handbook of Mathematical Functions, Dover, 1965.
[43] D. Wood, Phys. Rev. Lett. 46 (1981) 11.
[44] Y. He, T. Zeng, J. Phys. Chem. C 114 (2010) 18023.
[45] G. Mie, Ann. Phys. 25 (1908) 377.
[46] K. Ladutenko, U. Pal, A. Rivera, O. Pea-Rodríguez, Comput. Phys. Comm. 214 (2017) 225.
[47] S. Link, M.A. El-Sayed, J. Phys. Chem. B 103 (1999) 4212.
[48] C.E. Talley, J.B. Jackson, C. Oubre, N.K. Grady, C.W. Hollars, S.M. Lane, T.R. Huser, P. Nordlander, N.J. Halas, Nano Lett. 5 (2005) 1569.
[49] http://www.comsol.com.
[50] A. Deraemaeker, I. Babuška, P. Bouillard, Internat. J. Numer. Methods Engrg. 46 (1999) 471.
[51] H.Y. Ramírez, A. Santana, Comput. Phys. Comm. 183 (2012) 1654.
[52] K. Kluczyk, W. Jacak, J. Quant. Spectrosc. Rad. 168 (2016) 78.
[53] P.B. Johnson, R.W. Christy, Phys. Rev. B 6 (1975) 4370.
[54] S.O. Kasap, Principles of Electronic Materials and Devices, second ed., McGraw-Hill, 2002.
[55] R.C. Monreal, T.J. Antosiewicz, S.P. Apell, New J. Phys. 15 (2013) 083044.